Thermochimica Acta, 78 (1984) 29–38
Elsevier Science Publishers B.V., Amsterdam – Printed in The Netherlands

THERMAL DECOMPOSITION AND CREATION OF REACTIVE SOLID SURFACES. I. CHARACTERIZATION OF THE DECOMPOSITION PRODUCTS OF ALKALINE EARTH OXALATES

M.I. ZAKI * and M. ABDEL-KHALIK **

Chemistry Department, Faculty of Science, Minia University, El-Minia (Egypt)

(Received 24 January 1984)

ABSTRACT

Physicochemical characterization of the thermal decomposition products of $MgC_2O_4 \cdot 2\,H_2O$, $CaC_2O_4 \cdot H_2O$ or $BaC_2O_4 \cdot 0.5\,H_2O$ have been performed with the help of DTA, TGA, IRA and XRD analyses. Mechanisms for the solid-state decomposition reactions as well as corresponding activation energy values calculated according to a thermogravimetric method have been reported.

INTRODUCTION

As a matter of fact, it is relatively easy to produce inorganic solids of a particular composition but reactive-solid precursors must yield a product that not only has the correct composition but also possesses the proper physical attributes [1]. Thermal activation of simple reactive-solid precursors proceeds through decomposition solid-state reactions, viz. $P_s = R_s + X_g$. In this context, it can be inferred that topochemical processes may play the dominant role [2]. Such processes may lead to reactions in which the morphology of the product is a result of the existence of special fast transport paths (viz. surfaces, pores, grain boundaries and the surrounding gas atmosphere [3]). Hence, thermal decomposition normally leaves an oxide or metal which possesses pores, lattice imperfections and other characteristics that are necessary for its function as a reactive solid.

The present investigation concerns the thermal decomposition and textural consequences of some alkaline earth oxalates, viz. $MgC_2O_4 \cdot 2\,H_2O$, $CaC_2O_4 \cdot H_2O$ and $BaC_2O_4 \cdot 0.5\,H_2O$. They are economical reactive-oxide precursors (MgO, CaO, and BaO respectively [4]). This first part of this study, however, is confined to demonstrating and discussing results of

* To whom all correspondence should be addressed.
** Chemistry Department, Faculty of Science, Ain Shams University, Cairo, Egypt.

0040-6031/84/$03.00

physicochemical characterisation of the products obtained throughout the course of the thermal decomposition.

EXPERIMENTAL

The aimed physicochemical characterisation of the thermal decomposition products of the oxalates concerned (high-purity Merck products) was performed with the help of differential thermal (DTA), thermogravimetric (TGA), X-ray diffraction (XRD), and infrared absorption (IRA) analyses. The apparatus used and techniques adopted are reported in detail earlier [5].

The effect of the rate of heating (5, 10, 20, 30 or 50 °C min^{-1}) on the decomposition of the oxalates was investigated with the intention to calculate the activation energy values for each of the individual steps involved throughout the overall process according to the thermogravimetric method proposed by Ozawa [6].

RESULTS AND DISCUSSION

Results of the present investigation are graphically represented in Figs. 1–5, and partly given in Table 1. Figures 1 and 2 demonstrate TG and DTA curves automatically recorded over the range from room temperature (RT) up to 1300 °C, at a heating rate of 20 °C min^{-1}, and in a dynamic atmosphere of air (15 ml min^{-1}). Figure 3 shows XRD patterns calculated from corresponding powder diagrams. On the other hand, Figs. 4 and 5 display IR absorption spectra recorded over the range 4000–200 cm^{-1} at a resolution of 2.3 cm^{-1}. Table 1 gives the activation energy values (kcal mol^{-1}) calculated for the corresponding solid-state processes.

$MgC_2O_4 \cdot 2\ H_2O$

The TG curve given in Fig. 1C shows that the parent oxalate loses weight on heating in three steps. The first (110–150 °C) accounts for a very mild loss of ca. 1.5%. It is simultaneously accompanied by a very weak endothermic effect at 140 °C (Fig. 2C). The IR spectrum given (Fig. 4) for the parent-oxalate calcination product at 200 °C (for 3 h) shows a marked weakening of the absorptions at 2300, 680, 370 and 270 cm^{-1}. The low frequency absorptions (680–270 cm^{-1}) are usually assigned for vapour-like water molecules' vibrations [7], whereas the absorption at 2300 cm^{-1} is most likely to be a combination of the absorptions at 1620 and 680 cm^{-1}. Consequently, this early weight-loss step is related to the elimination of loosely bound (physically adsorbed) water.

The second step (160–220 °C) has been ascribed by Mourad and Nashed

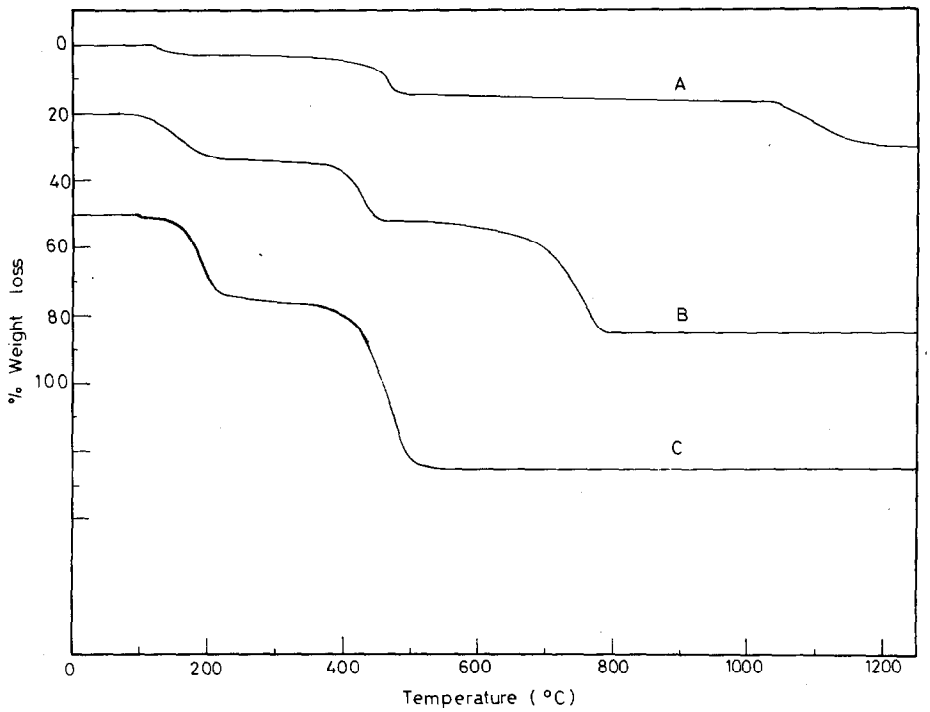

Fig. 1. TG curves for $BaC_2O_4 \cdot 0.5\ H_2O$ (A), $CaC_2O_4 \cdot H_2O$ (B), and $MgC_2O_4 \cdot 2\ H_2O$ (C).

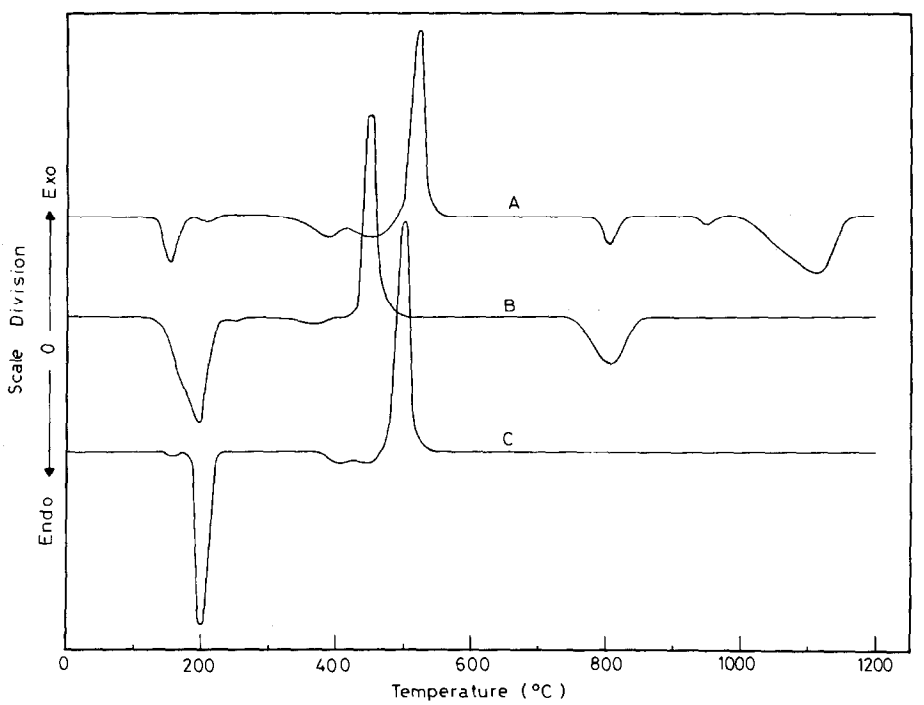

Fig. 2. DTA curves for $BaC_2O_4 \cdot 0.5\ H_2O$ (A), $CaC_2O_4 \cdot H_2O$ (B), and $MgC_2O_4 \cdot 2\ H_2O$ (C).

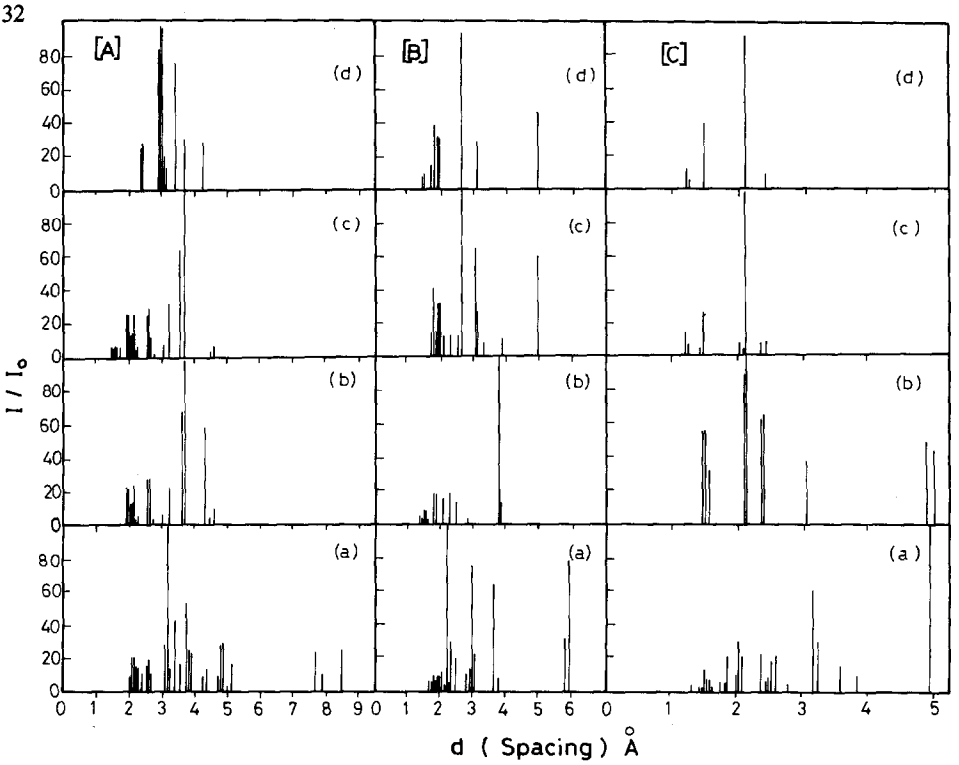

Fig. 3. XRD patterns for the parent materials (a) of (A) $BaC_2O_4 \cdot 0.5\ H_2O$, (B) $CaC_2O_4 \cdot H_2O$, and (C) $MgC_2O_4 \cdot 2\ H_2O$, and their calcination products at 500 (b), 800 (c), and 1200 °C (d) for 3 h.

TABLE 1

Solid-state processes involved in the overall decomposition of the alkaline earth oxalates concerned, and corresponding activation energy values calculated

Solid-state process	Temperature [a] (°C)	ΔE (kcal mol^{-1})
$MgC_2O_4 \cdot 2\ H_2O$		
$MgC_2O_4 \cdot 2\ H_2O \rightarrow MgC_2O_4 + 2\ H_2O$	160–220	16.9
$4\ MgC_2O_4 + 4\ H_2O + 0.5\ O_2 \rightarrow Mg_4(CO_3)_3(OH)_2 \cdot 3\ H_2O + 4\ CO$ $Mg_4(CO_3)_3(OH)_2 \cdot 3\ H_2O \rightarrow Mg_2CO_3(OH)_2 \cdot 3\ H_2O + 2\ MgO + 3\ CO_2 + 0.5\ O_2$ $Mg_2CO_3(OH)_2 \cdot 3\ H_2O \rightarrow 2\ MgO + 4\ H_2O + CO$	370–500	58.2
$CaC_2O_4 \cdot H_2O$		
$CaC_2O_4 \cdot H_2O \rightarrow CaC_2O_4 + H_2O$	150–210	13.2
$CaC_2O_4 \rightarrow CaCO_3 + CO$	360–430	54.2
$CaCO_3 \rightarrow CaO + CO_2$	570–820	59.5
$BaC_2O_4 \cdot 0.5\ H_2O$		
$BaC_2O_4 \cdot 0.5\ H_2O \rightarrow BaC_2O_4 + 0.5\ H_2O$	150–200	10.2
$BaC_2O_4 \rightarrow \alpha\text{-}BaC_2O_4 + CO$	390–490	58.2
$\alpha\text{-}BaCO_3 \rightarrow \beta\text{-}BaCO_3$	750–850	
$\beta\text{-}BaCO_3 \rightarrow \gamma\text{-}BaCO_3$	920–970	
$\gamma\text{-}BaCO_3 + 0.5\ O_2 \rightarrow BaO_2 + CO_2$	1020–1200	62.0

[a] Range at which the process occurs.

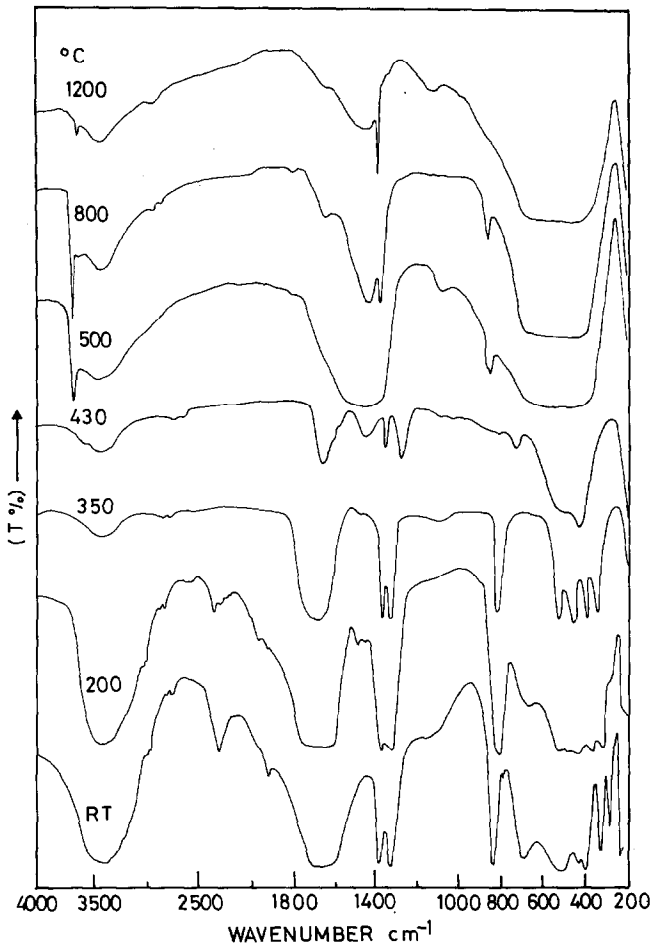

Fig. 4. IR spectra for the parent $MgC_2O_4 \cdot 2\,H_2O$ (RT) and its calcination products obtained at the temperatures indicated for 3 h.

[8] to the loss of the two molecules of crystallisation water. However, the way in which the step is graphically represented (Fig. 1C) shows that a continuous water loss occurs up to the take-over of the third step commencing at 370 °C. Relevant IR evidences can be easily reached on realizing the changes brought about by the spectrum of the calcination product at 350 °C (Fig. 4). The band structure exhibited is solely composed of absorptions normally assigned for different modes of inorganic oxalates' vibrations [9]. This, in turn, indicates a more or less complete disappearance of the absorptions at 3700–2900 and 700–400 cm^{-1} due to removal of crystallisation water [10]. In fact, water molecules have absorptions in the low-frequency region ($\leqslant$ 700 cm^{-1}), which arise from external motions, and torsional oscillations due to lattice effects are a reasonable cause [7]. Nevertheless, XRD patterns obtained for the calcination products at 200 or 350 °C reproduced the pattern

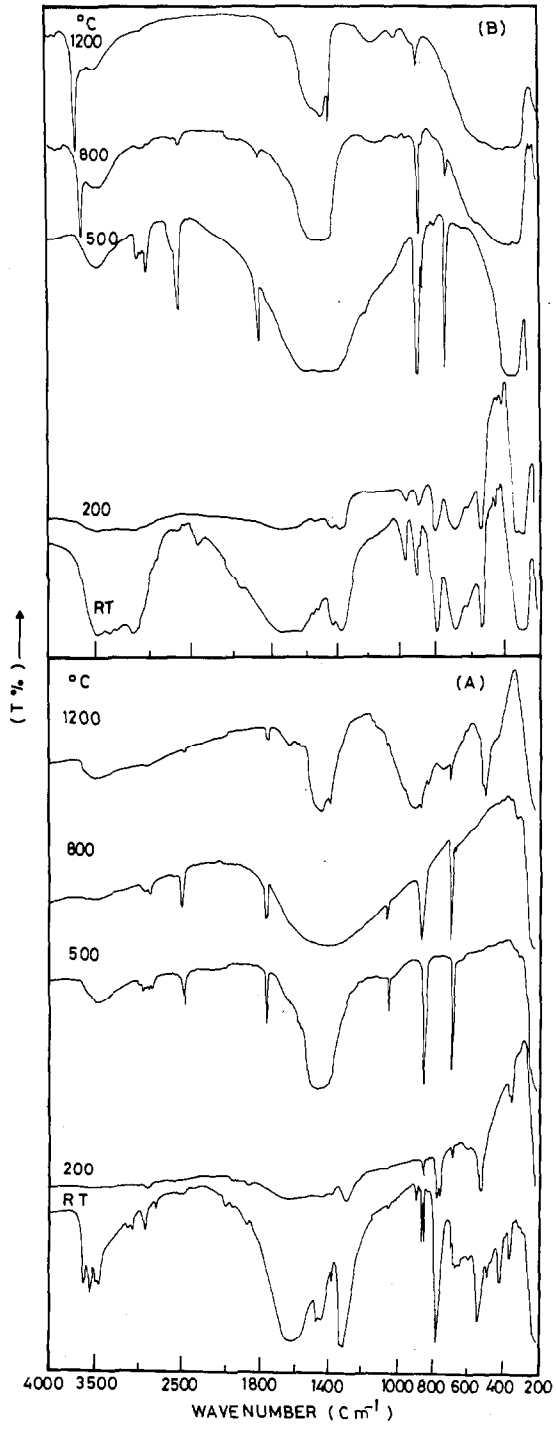

Fig. 5. IR spectra for parent (RT) and calcination products of (A) $BaC_2O_4 \cdot 0.5\ H_2O$, and (B) $CaC_2O_4 \cdot H_2O$, obtained at the temperatures indicated for 3 h.

shown for the hydrated parent oxalate. The concluded remarkable sensitivity of anhydrous magnesium oxalate for rehydration is strongly supported by kinetic results reported by Mourad and Nashed [8]. Accordingly [11,12] one may plausibly suggest that once the dehydration interface breaks through the interior of the material grains, the generated surface coordinatively unsaturated sites would dissociatively take up water molecules from those being driven off the bulk. The slow dehydration represented by the sloping plateau (220–360 °C) must, therefore, have occurred via a condensation-type process at the expense of surface hydroxyls.

The third weight-loss step commences at ca. 370 °C and ends at ca. 500 °C (Fig. 1C). The IR band structure exhibited (Fig. 4) for the 430 °C calcination product is composed of characteristic absorptions for both basic carbonate (at 3700–2900, 1600–1300, 1200–1100, 875 and 700–400 cm^{-1} [10]) and oxalate. The observed corresponding XRD pattern confirmed the existence of hydromagnesite, $Mg_4(CO_3)_3(OH)_2 \cdot 3\ H_2O$ (ASTM-card No. 8-179), as a major fraction and oxalate as a minor one.

On the other hand, the IR band structure exhibited (Fig. 4) for the calcination product at 500 °C conveys strong evidences for the lattice vibrations of MgO (vs absorption below 100 cm^{-1} [10]), free OH^- (s,sp absorption at 3700 cm^{-1}), and CO_3^{2-} (vs,b absorption at 1700–1200, 1070 and the doublet at 875 and 855 cm^{-1}). The relevant XRD pattern given for that calcination product (Fig. 3C) confirms the existence of highly dispersed MgO, as a major fraction, and traces of artinite, $Mg_2CO_3(OH)_2 \cdot 3\ H_2O$ (ASTM-card No. 6-0484). Therefore, the strong absorptions due to OH^- and CO_3^{2-} are consistent rather with surface species on MgO [13] than with bulk phases. Accordingly, the sloping plateau of the TG surve (Fig. 1C), at 500–800 °C, represents a slow simultaneous dehydration and decarbonation of relevant surface structures. On the other hand, the XRD patterns given (Fig. 3C) for products obtained at calcination temperatures $\geqslant$ 800 °C show no indications for any other bulk phases rather than MgO (ASTM-card No. 4-0829). The corresponding IR spectra (Fig. 4) display bands for surface species containing OH^- and/or CO_3^{2-}, though in small proportions, even after calcination at a temperature as high as 1200 °C. The strong exothermic effect located at 500 °C, as shown by the corresponding DT curve (Fig. 2C), is, therefore, associated rather with crystallisation of bulk MgO phase than of bulk carbonates [14].

The foregoing results suggest that the hydromagnesite, which is formed at the expense of the oxalate phase, decomposes giving MgO via the intermediate artinite. These transformations are conclusively formulated in the solid-state decomposition reactions compiled in Table 1. Corresponding activation energy values are also given in Table 1. It is worth mentioning that, based on the analysis of gaseous products, Rao and Ghandhe [15] detected the existence of CO and/or CO_2 at decomposition temperatures very compatible with the present results.

$CaC_2O_4 \cdot H_2O$

The TG curve given in Fig. 1B shows that $CaC_2O_4 \cdot H_2O$ loses weight along three steps. The first step commences (ca. 150 °C) where the elimination of physically adsorbed water is in progress (110–170 °C). This is reflected in a simultaneous composite endothermic effect (Fig. 2B) at 125–220 °C. Though the rate slows down remarkably at ca. 210 °C, the loss accompanied continues mildly until the commencement of the second step, at 360 °C. The total weight loss then inccurred amounts to 13.4%. According to results compiled elsewhere [16], the first step can be ascribed to the loss of the crystallisation water (12.3%). Consistent IR evidences are undoubtedly shown in the spectrum given (Fig. 5B) for the 200 °C calcination product. The characteristic absorptions displayed therein are solely due to different modes of anhydrous calcium oxalate vibrations [9]. Furthermore, the IR spectrum obtained for a calcination product at 350 °C, maintained the band structure of the anhydrous phase. The XRD pattern of this calcination product (350 °C) showed that CaC_2O_4 is much less sensitive for rehydration as compared to MgC_2O_4.

The second step commencing at 360 °C indicates that a weight loss of 21.5% is achieved at 430 °C. The product left shows a considerable thermal stability up to 570 °C. According to results compiled elsewhere [16], the strong exothermic effect, which interrupts (at 440 °C) the endothermic effect commencing at 360 °C could be ascribed to the transformation of "amorphous" to crystalline calcium carbonate. The XRD pattern given (Fig. 3B) for the calcination product obtained at 500 °C confirms the existence of bulk $CaCO_3$, as a sole product, crystallised in a calcite modification (ASTM-card No. 5-0453). Indeed, the absence of an IR absorption due to the symmetric stretch (ν_1), which usually occurs in the 1120–1040 cm^{-1} region [10], of carbonates in the spectrum given (Fig. 5B) for this calcination product could, in terms of symmetry considerations [17], lend a further support for the calcite modification.

The third weight-loss step at 570–820 °C (Fig. 1B) and the simultaneous endothermic effect at 800 °C (Fig. 2B) were ascribed to the decomposition of $CaCO_3$ leading to the formation of CaO [16]. In fact the weight loss recorded at 820 °C (43.5%) agrees favourably with that anticipated for such a decomposition process (44.0%). On the other hand, the XRD patterns given (Fig. 3B) for the calcination products obtained at $\geqslant$ 800 °C indicate the formation of bulk CaO (ASTM-card No. 4-0777) either as a dominant phase at 800 °C or as a sole phase at 1200 °C. Therefore, the IR absorptions usually assigned for free OH^- (at 3640 cm^{-1}) and CO_3^{2-} (at 2500, 1795, 1600–1300, 870 and 710 cm^{-1}), shown in the spectrum given (Fig. 5B) for the calcination product at 800 °C, are most probably due to relevant surface species on CaO [18,19]. Very much smaller proportions of such species are shown on CaO obtained at 1200 °C.

Table 1 compiles reaction equations suggested for the transformations involved throughout the course of the decomposition of the parent oxalate, together with corresponding activation energy values.

$BaC_2O_4 \cdot 0.5\ H_2O$

The IR spectrum given (Fig. 5A) for the parent-oxalate calcined at 200 °C declares a more or less complete pull out of the bands due to absorptions of different modes of both crystallisation and physisorbed water vibrations. In turn, this indicates that the first weight-loss step (110–200 °C) shown in the corresponding TG curve (Fig. 1A) leads to the formation of anhydrous BaC_2O_4. The XRD results indicated that anhydrous BaC_2O_4 has the least sensitivity for rehydration among the oxalates investigated in the present work.

On increasing the calcination temperature of the parent oxalate to 500 °C, i.e., just beyond the range at which the second weight-loss step occurs (390–490 °C), the product left has given rise to the characteristic IR bands of $BaCO_3$ [20]. The corresponding XRD pattern (Fig. 3A) confirms that this calcination product is solely composed out of bulk $BaCO_3$ of the aragonite-type of structure (α-phase; ASTM-card No. 5-0378). The absorption due to ν_1 shown in the corresponding IR spectrum at 1060 cm^{-1} is further evidence for the aragonite structure [10]. The strong exothermic effect at 500 °C (Fig. 2A) is, therefore, associated with the crystallisation of such a phase [21]. The TG curve shows that $BaCO_3$ thus obtained is thermally stable up to 1000 °C. This result was kinetically confirmed in an earlier investigation of the decomposition of $BaCO_3$ [22].

The endothermic effect at 810 °C (Fig. 2A), however, is ascribed to an $\alpha \rightarrow \beta$ polymorphic transformation [16]. Indeed, such a transformation can be confirmed by the consistent results given by both the IR spectrum (Fig. 5A) and the XRD pattern (Fig. 3A) obtained for the calcination product at 800 °C. A further $\beta \rightarrow \gamma$ polymorphic transformation has been assumed to take place just at the vicinity of the third weight-loss step commencing at 1020 °C; the endothermic effect at 950 °C is used as a monitor for it [16]. The third step and the simultaneous endothermic effect at 1120 °C are ascribed to the decomposition of $BaCO_3$ leading to the formation of BaO at 1200 °C. However, the XRD pattern given (Fig. 3A) for the calcination product at 1200 °C does not match that of BaO (ASTM-card No. 1-0746). It was indicated [23] that the strong IR absorptions shown in the spectrum of this calcination product, at 1000–800 and 550–450 cm^{-1}, are, respectively, due to symmetric stretches (ν_1) and torsional oscillations (ν_τ) of O_2^{2-} species. Therefore, the formation of BaO_2 may be presumed at this stage. The higher heat of formation reported [24] for BaO_2 (635.9×10^{-6} J kg^{-1} mol^{-1}) as compared to that for BaO (553.1×10^{-6} J kg^{-1} mol^{-1}) may lend a thermodynamic support for such a presumption.

REFERENCES

1 N.H. Brett, K.J.D. MacKenzie and J.H. Sharp, Q. Rev. Chem. Soc., 24 (1970) 185.
2 D.A. Young, Decomposition of Solids, Pergamon Press, Oxford, 1966.
3 H. Schmalzried, Solid State Reactions, 2nd edn., Verlag Chemie, Weinheim, 1981, pp. 190–199.
4 G.V. Samsonov, The Oxide Handbook, IFI/Plenum, New York, 1973, pp. 411–452.
5 R.B. Fahim, M.I. Zaki and R.M. Gabr, Surf. Technol., 11 (1980) 215.
6 T. Ozawa, Thermal Analysis Application Data, Scientific Publications of Shimadzu Corporation, Japan, Ser. No. 3010-04901, p. 10.
7 F.A. Miller, G.L. Carlson, F.F. Bentley and W.H. Jones, Spectrochim. Acta, 16 (1959) 135.
8 W.E. Mourad and S. Nashed, Thermochim. Acta, 41 (1980) 117.
9 K. Nakamoto, Infrared and Raman Spectra of Inorganic and Coordination Compounds, 3rd edn., Wiley, New York, 1978, pp. 233–237.
10 J.A. Gadsden, Infrared Spectra of Minerals and Related Inorganic Compounds, Butterworths, London, 1975, p. 16.
11 R.B. Fahim, M.I. Zaki and N.H. Yacoub, J. Chem. Soc., Faraday Trans. 1, 78 (1982) 2721.
12 A.C. Zettlemoyer and E. McCafferty, Croat. Chem. Acta, 45 (1973) 173.
13 M.W. Roberts and J.M. Thomas (Senior Reporters), Specialist Periodical Report, Surface and Defect Properties of Solids, Vol. 2, The Chemical Society, London, 1973, pp. 116–118.
14 R.M. Dell and V.J. Wheeler, 5th Int. Symp. React. Solids, Munich, 1965, pp. 343–360.
15 T.S. Rao and B.R. Ghandhe, J. Chromatogr., 88 (1974) 707.
16 G. Liptay, Atlas of Thermoanalytical Curves, Heyden, London, Vol. 1, 1971, Vol. 2, 1973.
17 H.H. Adler and P.F. Kerr, Am. Mineral., 48 (1963) 839.
18 M.J.D. Low, N. Tkezawa and A.J. Goodsel, J. Colloid Interface Sci., 37 (1971) 422.
19 N.E. Tretyakov and V.N. Filimonov, J. Kinet. Catal. (U.S.S.R.), 11 (1970) 815.
20 F.A. Miller and C.H. Wilkins, Anal. Chem., 24 (1952) 1253.
21 J. Paulik, F. Paulik and L. Erdey, Anal. Chim. Acta, 44 (1969) 153.
22 R.B. Fahim, M.I. Zaki and G.A.M. Hussien, Powder Technol., 33 (1982) 161.
23 N. Sheppard, personal communication, 1983.
24 G.V. Samsonov, The Oxide Handbook, IFI/Plenum, New York, 1973, p. 40.